



HAL
open science

SMOS salinity in the subtropical North Atlantic salinity maximum: 1. Comparison with Aquarius and in situ salinity

Olga Hernandez, Jacqueline Boutin, Nicolas N. Kolodziejczyk, Gilles Reverdin, Nicolas Martin, Fabienne Gaillard, Nicolas Reul, Jean-Luc Vergely

► To cite this version:

Olga Hernandez, Jacqueline Boutin, Nicolas N. Kolodziejczyk, Gilles Reverdin, Nicolas Martin, et al.. SMOS salinity in the subtropical North Atlantic salinity maximum: 1. Comparison with Aquarius and in situ salinity. *Journal of Geophysical Research*, 2014, 119 (12), pp.8878-8896. 10.1002/2013JC009610 . hal-01131556

HAL Id: hal-01131556

<https://hal.science/hal-01131556>

Submitted on 22 Oct 2021

HAL is a multi-disciplinary open access archive for the deposit and dissemination of scientific research documents, whether they are published or not. The documents may come from teaching and research institutions in France or abroad, or from public or private research centers.

L'archive ouverte pluridisciplinaire **HAL**, est destinée au dépôt et à la diffusion de documents scientifiques de niveau recherche, publiés ou non, émanant des établissements d'enseignement et de recherche français ou étrangers, des laboratoires publics ou privés.

RESEARCH ARTICLE

10.1002/2013JC009610

Companion to *Kolodziejczyk et al.*
[2015], doi:10.1002/2014JC010103.

Special Section:

Early Scientific Results from
the Salinity Measuring
Satellites Aquarius/SAC-D
and SMOS

Key Points:

- SMOS salinity validated in the subtropical North Atlantic Ocean
- 39 transects of ships SSS collocated with SMOS and AQUARIUS SSS data
- Advantage of SMOS over ARGO and AQUARIUS to sample SSS mesoscale features

Correspondence to:

O. Hernandez,
olgahernand@gmail.com

Citation:

Hernandez, O., J. Boutin, N. Kolodziejczyk, G. Reverdin, N. Martin, F. Gaillard, N. Reul, and J. L. Vergely (2014), SMOS salinity in the subtropical North Atlantic salinity maximum: 1. Comparison with Aquarius and in situ salinity, *J. Geophys. Res. Oceans*, 119, 8878–8896, doi:10.1002/2013JC009610.

Received 19 NOV 2013

Accepted 19 JUN 2014

Accepted article online 25 JUN 2014

Published online 26 DEC 2014

SMOS salinity in the subtropical North Atlantic salinity maximum: 1. Comparison with Aquarius and in situ salinity

O. Hernandez¹, J. Boutin¹, N. Kolodziejczyk¹, G. Reverdin¹, N. Martin¹, F. Gaillard²,
N. Reul³, and J. L. Vergely⁴¹LOCEAN/IPSL, Paris, France, ²LPO/IFREMER, Brest, France, ³LOS/IFREMER, Toulon, France, ⁴ACRI-ST, Paris, France

Abstract Sea surface salinity (SSS) measured from space by the Soil Moisture and Ocean Salinity (SMOS) mission is validated in the subtropical North Atlantic Ocean. 39 transects of ships of opportunity equipped with thermosalinographs (TSG) crossed that region from 2010 to 2012, providing a large database of ground truth SSS. SMOS SSS is also compared to Aquarius SSS. Large seasonal biases remain in SMOS and Aquarius SSS. In order to look at the capability of satellite SSS to monitor spatial variability, especially at scales less than 300 km (not monitored with the Argo network), we first apply a monthly bias correction derived from satellite SSS and In Situ Analysis System (ISAS) SSS differences averaged over the studied region. Ship SSS averaged over 25 km is compared with satellite and ISAS SSS. Similar statistics are obtained for SMOS, Aquarius, and ISAS products (root mean square error of about 0.15 and global correlation coefficient r of about 0.92). However, in the above statistics, SSS varies due to both large-scale and mesoscale (here for scales around 100 km) variability. In order to focus on mesoscale variability, we consider SSS anomalies with respect to a monthly climatology. SMOS SSS and Aquarius SSS anomalies are more significantly correlated ($r > 0.5$) to TSG SSS anomaly than ISAS. We show the effective gain of resolution and coverage provided by the satellite products over the interpolated in situ data. We also show the advantage of SMOS ($r = 0.57$) over Aquarius ($r = 0.52$) to reproduce SSS mesoscale features.

1. Introduction

During the last decades, the global change in freshwater balance is responsible for the increase in Sea Surface Salinity (SSS) in North Subtropical Atlantic [Curry *et al.*, 2003; Gordon and Giulivi, 2008]. This region is characterized by strong evaporation and intense seasonal surface heating and displays the highest salinity values worldwide in the open ocean [Boyer and Levitus, 2002; Bingham *et al.*, 2012]. The SSS is forced at all scales by evaporation and precipitation [e.g., Lagerloef *et al.*, 2010; Reul *et al.*, 2013; Boutin *et al.*, 2013]; continental freshwater input [e.g., Dai and Trenberth, 2002]; vertical mixing with subsurface water masses [e.g., Kolodziejczyk and Gaillard, 2013]; and horizontal advection of salinity [e.g., Reverdin *et al.*, 2007]. This emphasizes the need for well-sampled SSS data in order to get more insight in the SSS spatiotemporal variability and the respective role of the different forcing on the SSS change.

Until now, the best spatiotemporal coverage of the SSS field was provided by the Argo array of autonomous profiling floats with more than 3500 active floats (<http://www.coriolis.eu.org>) deployed over the global ocean. The Argo floats perform one profile of temperature and salinity from 2000 m to the surface (~5 m) every 10 days. On average over the whole ocean, they provide about one SSS measurement every 10 days and every $3^\circ \times 3^\circ$. However, this resolution is still too coarse to resolve important temporal and spatial scales over which Sea Surface Salinity (SSS) is known to vary significantly [Delcroix *et al.*, 2005; Lagerloef *et al.*, 2010; Reul *et al.*, 2013].

Complementary to the in situ measurements, new satellite SSS is provided by the Soil Moisture and Ocean Salinity (SMOS) mission (European Space Agency's water mission) launched in November 2009 [Mecklenburg *et al.*, 2012] and Aquarius/SAC-D mission launched in June 2011 [Lagerloef *et al.*, 2008; Lagerloef, 2012]. For the first time, these new SSS measurements allow to obtain consistent global maps of SSS from satellite [Kerr *et al.*, 2010; Font *et al.*, 2010]. The goal of the SMOS and Aquarius mission is to provide SSS with an accuracy of about 0.1–0.2 on average over GODAE (Global Ocean Data Assimilation Experiment) scale ($100 \times 100 \text{ km}^2$ over 1 month). Quality assessment of the SMOS SSS products averaged over $100 \times$

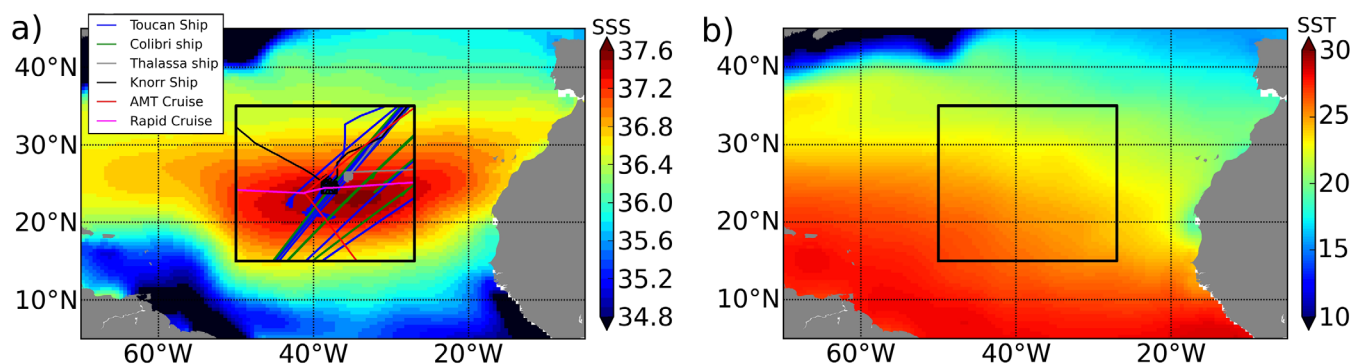


Figure 1. (a) Annual mean SSS from ISAS climatology. Transects from MN Toucan (17 transects), MN Colibri (18 transects), RV Thalassa, RV Knorr, AMT cruise, and Rapid cruise are superimposed. (b) Annual mean SST from ISAS climatology. The black rectangle shows the study region: 50°W–27°W, 15°N–35°N.

100 km² and 10 days revealed an accuracy of about 0.3–0.4 in the tropical and subtropical regions and about 0.5 in the more poleward regions [Boutin *et al.*, 2013; Reul *et al.*, 2013]. This latitudinal dependency of the satellite microwave SSS accuracy is mainly due to the change of SMOS brightness temperature sensitivity to salinity with sea surface temperature. The latter reaches a maximum in warm waters (0.7 K for a variation of 1 in SSS at SST = 30°C) and strongly decreases in cold ones (0.2 K for a variation of 1 in SSS at SST = 0°C) [Klein and Swift, 1977]. The warm region of the Atlantic subtropical salinity maximum is thus optimally suited to test and validate the capability of the satellites at retrieving the SSS variability.

In this study, the SMOS SSS data are validated in the subtropical North Atlantic salinity maximum region (Figure 1) by comparison with in situ data over the period July 2010 to December 2012, at spatial scales varying from 1000 to 100 km (referred to as mesoscale). This is the region of the SPURS (Salinity Processes in the Upper Ocean Regional Study) experimental program (see <http://spurs.jpl.nasa.gov/SPURS>). In order to allow comparison with in situ data at such scales, we take advantage of the transects of high-resolution (~2.5 km) thermosalinograph SSS measurements from the SPURS/Strasse cruises. The transects are repeated several times a year across the maximum SSS region of North Atlantic between July 2010 and December 2012. We also compare in situ SSS data with Aquarius Level 3 SSS products and with an optimal interpolation of in situ (mainly Argo) data (ISAS).

After a description of data and methods, we present precise collocations of SMOS SSS with in situ ship SSS. In section 4.2, TSG data are compared with SMOS, Aquarius, and ISAS monthly products. In section 4.3, the mesoscale SSS features retrieved in SMOS and Aquarius are evidenced. The results are discussed and summarized in the last section.

2. Data

2.1. In situ Data

2.1.1. In situ Analysis System (ISAS) SSS

In this study, we use the monthly fields of salinity ISAS-13 [Gaillard, 2012], available for the period 2002–2012 that overlap the SMOS measurements period 2010–2012, and the monthly climatology ISAS-13 (resulting from an average of ISAS-13 analyzed fields over 2004–2012). They were obtained with ISAS (In Situ Analysis System) version 6, an optimal estimation tool designed for the synthesis of the Argo global data set [Gaillard *et al.*, 2009].

The interpolated fields were produced over the global ocean by the ISAS project with data sets downloaded from the Coriolis data center. The field of analysis has a global coverage within 70°S–70°N.

The optimal interpolation is computed over a 1/2° grid and involves a structure function modeled as the sum of two Gaussian functions, each associated with specific time and space scales, resulting in the open ocean subtropics, in a smoothing close to 300 km [for details, see Gaillard *et al.*, 2009]. In our study, these fields have been interpolated linearly onto a regular 0.25° grid. This interpolation is not expected to bring

any new information with respect to the original ISAS field about small-scale structures and is only intended to facilitate the comparisons with other fields produced at this spatial scale.

The temperature and salinity fields are reconstructed on 152 levels ranging from 0 to 2000 m depth. We used the first level that mostly referred to the shallowest valid Argo measurement between the surface and about 5 m depth. The major contribution to ISAS is the profiling floats from the Argo array. This data subset is complemented by data from the Tropical Moored Buoy Array program (TAO/TRITON (Tropical Atmosphere Ocean/Triangle Trans-Ocean Buoy Network), PIRATA (Prediction and Research Moored Array in the Atlantic), RAMA (Research Moored Array for African-Asian-Australian Monsoon Analysis and Prediction)) mooring array. A few CTD profiles transmitted in real time are used but XBTs and X-CTDs were excluded from the analysis because of uncertainties in the fall rate.

2.1.2. SSS Ship

In situ near-surface salinity is provided by thermosalinographs (TSG) mounted on the merchant vessels Toucan and Colibri that cross the North Atlantic subtropical sea surface salinity maximum (SSM). These measurements onboard ships of opportunity are a contribution to French Sea Surface Salinity Observation Service (<http://www.legos.obs.mip.fr/observations/sss>). 39 transects with salinity data have been collected between 2010 and 2012 from Western Europe to northern South America (Figure 1 and Table A1). The near-surface seawater is pumped on the side of the immersed ship's hull at about 5 m depth. The nominal horizontal resolution is about 2.5 km. The typical duration of ship transect between Europe and South America is 10 days for each ship. Data are systematically postcalibrated with water samples and Argo data when they are available. Only data with "Adjusted" and "Good" or "Probably Good" flags data are used in this study (<http://www.legos.obs.mip.fr/observations/sss/datadelivery/dmdata>). The typical error on these TSG measurements is 0.01–0.02; on the crossings used in our study the difference between the calibrated TSG salinities and the water sample salinities vary between 0.01 and 0.08, part of this difference being possibly due to errors in the water sample salinities.

TSG data were also available from the research vessel (RV) Thalassa (Figure 1) during the STRASSE (SubTropical Atlantic Surface Salinity Experiment) cruise, from the RV Knorr during the SPURS-1 (Salinity Processes in the Upper Ocean Regional Study) cruise, from the RV Discovery (Di382) during the RAPID cruise [McCarthy *et al.* 2012] and from the RRS James Cook (JC079) during the AMT 22 (Atlantic Meridional Transect) cruise. Salinity of these cruise data has been validated with errors on the order of 0.005. We adopt the practical salinity scale (pss-78), defining salinity as a conductivity ratio, which does not have physical units.

2.2. Satellite Data

2.2.1. SMOS Data

SMOS satellite was launched in November 2009 into a sun-synchronous orbit at 758 km crossing the equator twice a day at 6 A.M. in ascending phase and at 6 P.M. in descending phase [Mecklenburg *et al.*, 2012]. The SMOS mission carries the L-band (1.4 GHz) Microwave Imaging Radiometer with Aperture Synthesis (MIRAS) instrument from which a bidimensional field of view (FOV) of brightness temperatures (T_b) at various incidence angles is reconstructed. SMOS SSS considered in this paper is based on T_b measurements at less than 300 km from the satellite center track. Coverage of the global ocean is achieved every 3 days with a repeat cycle of 149 days (subcycle of 18 days) and a nominal spatial resolution of 43 km on average over the FOV.

We first use the SMOS ESA L2 SSS, reprocessed using ESA version 5 processors. In this reprocessing, an "Ocean Target Transformation" (OTT) correction was applied every 2 weeks. This correction aims at correcting SMOS brightness temperatures (T_b) from systematic differences with respect to modeled T_b in the FOV [Yin *et al.*, 2012]. It is computed from a large oceanic region far from land and a Radio Frequency Interference (RFI) contamination between 45°S and 5°S in the eastern Pacific [Yin *et al.*, 2013]. However, seasonal and latitudinal biases are still present. Attempts to reduce such biases (including improved SMOS raw data calibration as well as the use of a time-varying OTT) remain under study [Martin-Neira *et al.*, 2013; Yin *et al.*, 2013].

SMOS SSS and their theoretical errors are retrieved from multi-incidence brightness temperatures (T_bs) collected at an earth pixel during the satellite pass, using Levenberg-Marquard (L.M.) minimization method as described in Zine *et al.* [2008], after adjusting direct models with SMOS measurements (see a complete description in the Algorithm Theoretical Basis Document (ATBD) available at: <http://www.argans.co.uk>).

Table 1. Summary of Characteristics of SMOS CATDS-CEC SSS Level 3 Products^a

	SMOS CATDS CEC LOCEAN	SMOS CATDS CEC IFREMER
SSS method retrieval	SSS retrieved from polarized Tbs along dwell lines using an iterative retrieval (see ESA L2OS ATBD)	SSS retrieved from first Stokes parameter [Reul and Tenerelli, 2011]
Region of the instrument field of view (FOV) considered for SSS	Alias Free Field of View (AFFOV) and extended AFFOV along dwell lines with at least 130 Tb in AFFOV ($\sim \pm 300$ km from the swath center)	Alias Free Field of View only
Tb sortings	Determined from consistency along dwell lines as reported in ESA Level 2 products	Determined from interorbit consistency in incidence angles classes and thresholding
Galactic model	Kirchoff Approx. scattering at 3 m/s	Geometrical optics model
Wind model	Model 1 (Empirical adjustment of parameters in roughness model and foam coverage models [Yin et al., 2012])	Model 2 (Empirical adjustment of Tb dependencies to wind speed by using bin average)
Calibration	Variable OTT (every 2 weeks synchronised with Noise Injection Radiometer as defined in ESA reprocessing)	Single Ocean Target Transformation (OTT) + daily $5\bar{r} \times 5\bar{r}$ adjustment wrt World Ocean 2001 SSS climatology
Grid resolution	Averaged over 100×100 km ² and oversampled every 0.25°	Averaged over 50×50 km ²
Averaging method	Average weighted by theoretical error on retrieved SSS and spatial resolution	Simple average

^aTable adapted from Reul et al. [2013].

The theoretical error is retrieved from the Jacobian of Tb with respect to the geophysical parameters and from the a posteriori covariance matrix of errors in Tb and geophysical parameters [see Zine et al., 2008]. To first order, the theoretical error depends on the number of Tb data used in the SSS retrieval and on Sea Surface Temperature (SST; because of the strong dependency of dTb/dSSS with SST). Relative accuracy of these SMOS data has been estimated as ~ 0.3 – 0.5 or better in tropical and subtropical regions for SSS averaged over 100×100 km² and 10 days [Boutin et al., 2013].

The Level 3 product named SMOS CATDS CEC LOCEAN_v2013 has been generated from the above ESA Level 2 v5 reprocessed products (L2OS v5 wind-model 1; see Table 1), using only retrievals performed under moderate wind speed (3 – 12 m s⁻¹) and according to the flags described in Boutin et al. [2013], except that the galactic noise flag was not tested (data affected by large galactic noise are nevertheless sorted out), and land mask is only 40 km. Level 3 SSS is flagged and averaged over 1 month, 100×100 km² and oversampled every 0.25°. When averaging Level 2 SSS, each retrieved SSS is weighted by its spatial resolution and its theoretical uncertainty as derived by the L.M. algorithm (for more details see Yin et al. [2012]).

Two other LOCEAN products were built for the purpose of this study. First, a SMOS LOCEAN 0.25° product is averaged following the same method as SMOS CATDS CEC LOCEAN maps, but the average is performed over $0.25^\circ \times 0.25^\circ$ instead of 100×100 km². Second, a SMOS LOCEAN OI is produced from SMOS LOCEAN 0.5° product optimally interpolated with a similar method and same spatial correlation lengths as the one applied by ISAS [see Gaillard et al., 2009].

Apart from the Level 2 iterative L.M. retrieval, the IFREMER expertise center of CATDS (Centre Aval de Traitement des données SMOS, www.catds.fr) has developed an alternative processing chain starting from Level 1B products, in which the retrieval is simpler (SSS is retrieved from the first Stokes parameter, wind speed is not retrieved), RFI filtering is more efficient, only one OTT is applied over the whole period and a large-scale bias correction is applied. A more complete comparison of the two Level 3 products we consider is given in Table 1. We use monthly SMOS-CATDS CEC IFREMER SSS maps, averaged over 50×50 km² and oversampled every 0.25° with a daily $5^\circ \times 5^\circ$ adjustment with respect to World Ocean 2001 climatology. In this product, RFI percentage is estimated at each pixel. Only pixels for which the RFI percentage is null are used in this study. Nevertheless, undetected small amplitude residual contamination possibly remains in the data.

Our study focuses on the period July 2010 to December 2012. In December 2010, the last week of the month was not sampled due to an electrical stability test aboard the SMOS satellite. In January 2011, the

three first weeks were degraded due to problems on one satellite arm (http://earth.eo.esa.int/missions/smos/available_data_processing.html). For these reasons, December 2010 and January 2011 are excluded from the analysis.

2.2.2. Aquarius Data

The Aquarius satellite was launched in June 2011 into a polar sun-synchronous orbit at 657 km crossing the equator twice a day at 6 P.M. in ascending phase (Orbit A) and at 6 A.M. in descending phase (Orbit D). It carries out a microwave radiometer at 1.413 GHz along with a scatterometer at 1.26 GHz for surface roughness correction. The nominal resolution of Aquarius satellite is about 100 km with a 7 days global coverage.

As for SMOS, several Level 3 products are available depending on the processing made. Here we use the two latest Level 3 versions of Aquarius data released to the scientific community (<http://podaac.jpl.nasa.gov/datasetlist?search=aquarius>): the Aquarius version 2.0 (see Aquarius Algorithm Theoretical Basis Documents (ATBD)) [Wentz and Le Vine, 2012; Lagerloef et al., 2013] and the Aquarius CAP version 2.0 [Yueh et al., 2012]. For both versions, we use the monthly spatial maps at 1° spatial resolution. In the Aquarius V2 CAP version, SSS is retrieved with the Combined Active Passive (CAP) algorithm which utilizes simultaneously data from the on board radiometer and scatterometer to retrieve SSS, wind speed, and direction by minimizing the sum of squared differences between model and observations. We have performed some tests with the temporary version V2.5.1, which is precursor of the new version 3.0 that should be released in spring 2014. Although large-scale biases were reduced, we could not evidence improvement in the detection of mesoscale features, so that we prefer to keep the V2.0 official version.

3. Methods

3.1. Definition of the Region Under Study

The goal of our study is to evaluate SMOS and Aquarius performances over the open ocean. Hence, we first conduct a preliminary study to avoid regions strongly contaminated by continent vicinity and by RFI. We define our region based on these criteria. Land contamination varies depending on the location of the pixel across track [Vergely et al., 2013]. Given that the orbit of SMOS is not repetitive over 1 month, land contamination is expected to generate artificial SSS variability, in addition to the already observed bias.

RFI sources vary in time both because the RFI emissions signals vary and because the contamination will depend on the location of the RFI contaminated point in the SMOS FOV. Hence, these contaminations are expected to artificially increase the SMOS brightness temperature variability, and hence the SSS variability observed within 1 month.

We estimate the variability of SMOS SSS retrieved along swath at about 40 km resolution within $100 \times 100 \text{ km}^2$ and 1 month from the standard deviation (σ) of SMOS L2 SSS. We define the natural variability of the SSS E_{var} in SMOS as:

$$E_{var} = \sqrt{\sigma^2 - E_{th}^2} \quad (1)$$

where σ^2 is the total variance of SMOS SSS, including natural variability, variability due to pollution sources (RFI, land contamination), and the theoretical error E_{th} of the retrieved SSS related to radiometric noise and uncertainties of auxiliary parameters used in the retrieval. Thus, in case of no external pollution sources, we expect that E_{var} is the natural variability retrieved from SMOS SSS.

Figures 2a and 2b show the quadratic means of σ and E_{var} , respectively, over the period July 2010 to December 2012. σ is higher than 0.6 everywhere, a large part comes from the radiometric noise: E_{th} in this region ranges from 0.5 to 0.8. On ship SSS, we always observe natural variability along 100 km to be lower than 0.4. Unrealistically, high values of E_{var} are observed close to continents and in the northern region where RFI is expected. Therefore, we decide to bound the region under study to 50°W to 27°W in longitude and to 15°N to 35°N in latitude. This region will be referred to as the North Subtropical Atlantic (NSA).

In January 2012, we observe large anomalies between quadratic means of σ and expected theoretical error aligned with ascending orbits passes. By analyzing individual orbits, we observe abnormally low SMOS SSS (as low as 31) along ascending orbits from 26 to 29 January crossing the eastern part of our region.

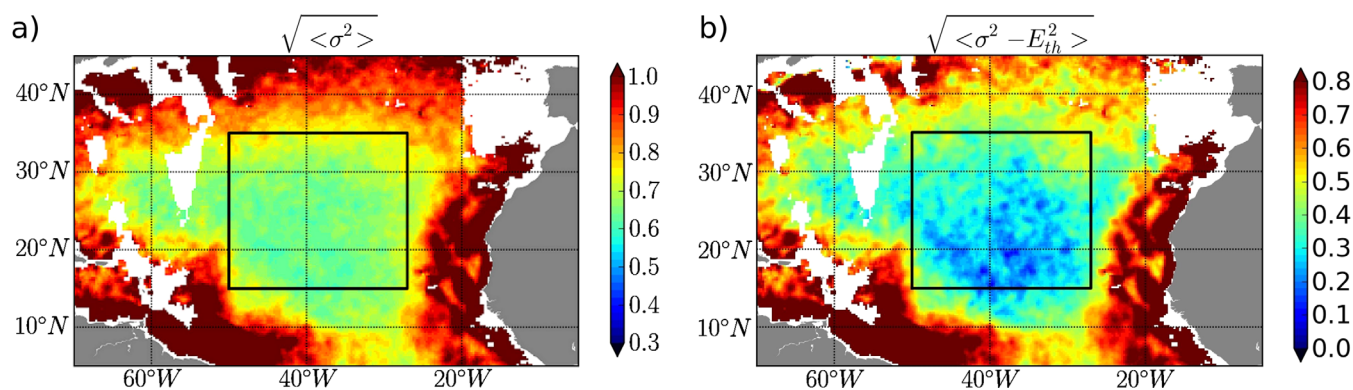


Figure 2. (a) Quadratic mean of σ , (b) quadratic mean of E_{var} , see equation (1). The black rectangle shows the study region: 50°W–27°W, 15°N–35°N.

These values were not filtered by SMOS flags but are likely due to RFI; hence in January, only the period of 1–26 January was retained in the monthly average.

3.2. Bias Corrections

Large-scale comparisons of regional averaged SSS maps show that the SSS seasonal variability in the NSA region calculated from SMOS and Aquarius is not consistent with observations (Figure 3a). SMOS CEC LOCEAN (black curves) and Aquarius (cyan and blue curves) do not consistently reproduce the seasonal variability shown in in situ data (red and magenta curves). SMOS CEC LOCEAN (black curves; Figures 3a and 3b) presents a very strong boreal winter bias (up to -0.4) that is visible each year, possibly due to strong sun contamination on descending orbits at that time. The SMOS CEC IFREMER reproduces the observed seasonal variability with ISAS products. However, this feature is expected because the IFREMER product is adjusted to the World Ocean Climatology (WOA 2001) [Conkright and Boyer, 2002] with a daily $5^\circ \times 5^\circ$ adjustment. Tests performed with Aquarius version 2.5.1 which is precursor of the future version 3 to be released soon, indicate that the large-scale seasonal biases are much reduced especially with CAPV2.5.1 (not shown).

The ISAS SSS products between 2010 and 2012 are saltier (about 0.1) than the climatological SSS seasonal cycle derived from WOA 2009. This is likely an effect of the long-term trend of increasing salinity in North Subtropical Atlantic during the last decade year [Reverdin et al., 2007; Gordon and Giulivi, 2008; Durack and Wijffels, 2010; Terray et al., 2012].

In order to study the spatial variability of SSS, we first correct both satellite data sets (SMOS and Aquarius) from a bias $B1$ (equation (2), Figure 3b) with respect to ISAS, estimated each month from an average in the NSA region (Figure 3b).

$$B1 = \langle SSS_{SAT} \rangle_{NSA} - \langle SSS_{ISAS} \rangle_{NSA} \quad (2)$$

where $\langle SSS_{SAT} \rangle_{NSA}$ is the satellite SSS averaged over the NSA region and $\langle SSS_{ISAS} \rangle_{NSA}$ is the ISAS SSS averaged over the NSA region.

3.3. Colocations and Statistics

Figure 4 summarizes the characteristics of the satellite products used in our colocations. Precise colocations between in situ data and SMOS data are performed by averaging Level 2 SMOS SSS at ± 50 km and ± 9 days, using the same flags as described in Boutin et al. [2013]. The ± 9 days are chosen to cover the 18 day SMOS repeat subcycle.

Statistics of the differences between satellite and in situ SSS were derived: mean bias error (MBE), the root mean square error (RMSE, equation (B3)), the correlation coefficient (r , (B1)), and the least squares fit. All correlation coefficients that we report are significantly nonzero at 99% interval confidence. To analyze the significance of the difference in correlation coefficients between the products, we use the fisher r-to-z

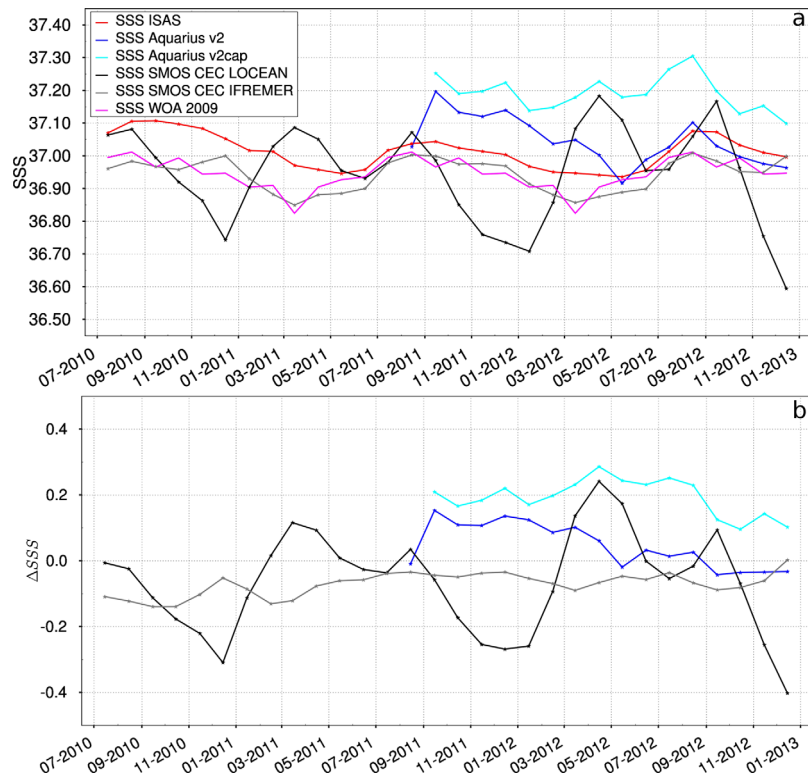


Figure 3. (a) SSS variability from SMOS and Aquarius satellite, ISAS data, and WOA 2009 climatology. (b) Bias B1 applied to all data sets.

transformation [Zar, 2010] (equation (B2)). We also calculate the standard deviation (σ , equation (B5)) of each satellite product (σ_p) and of in situ data (σ_o).

For the comparison with the Level 3 products, in order to be able to compare the statistics between the different SSS products, we regridded all SSS products onto a $0.25^\circ \times 0.25^\circ$ resolution grid and $1^\circ \times 1^\circ$ resolution grid (Table 2). The

gridding at 1° resolution is achieved by averaging the SSS values in $1^\circ \times 1^\circ$ cells, while the gridding at 0.25° resolution is achieved by oversampling the products using a bilinear interpolation. TSG data are averaged either at 0.25° or 1° resolution.

Statistics have been estimated during the overlapping period between SMOS and Aquarius (from September 2011 to December 2012). That period includes 21 ship SSS transects. We have checked that the obtained statistics for SMOS and ISAS were not significantly modified by using TSG data from July 2011 to December 2012. For all monthly satellite

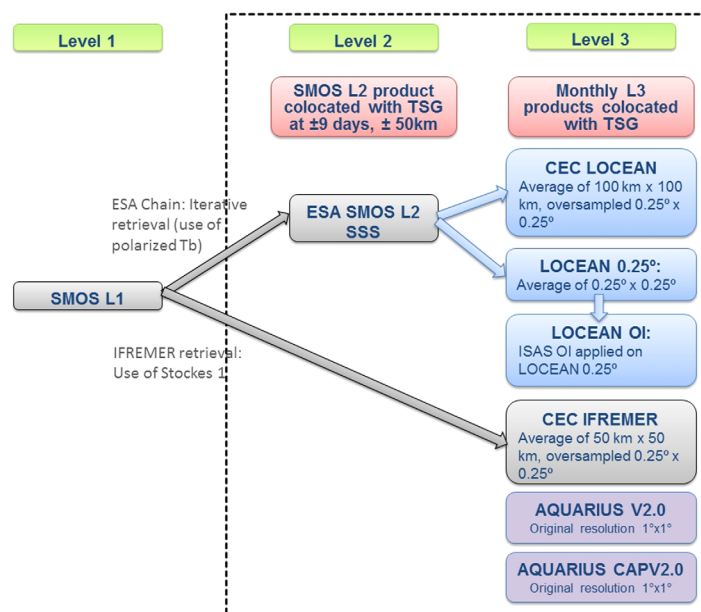


Figure 4. Summary of the different satellite data sets which are compared to in situ data.

Table 2. Statistics of Colocation of SMOS at ± 9 days and ± 50 km with TSG SSS^a

	r	MBE	RMSE	σ_{TSG}	σ_p
SSS SMOS AD—SSS TSG (not filtered)	0.886	0.00	0.18	0.38	0.38
SSS SMOS AD—SSS TSG (filtered)	0.897	0.01	0.17	0.37	0.38
SSS SMOS A—SSS TSG (filtered)	0.878	0.01	0.20	0.37	0.41
SSS SMOS D—SSS TSG (filtered)	0.722	0.04	0.26	0.37	0.41

^aThe number of values n is equal to 109781. “(filtered)” indicates that a running mean average at ± 50 km and ± 9 days was applied to TSG SSS: A for ascending orbits, D for descending orbits, AD for both ascending and descending orbits. Statistics of the second experiment is presented in Figure 6. Correlation coefficient is significant at 99%.

products, a combination of ascending and descending orbits was used. In these comparisons we did not take into account uncertainty on TSG data nor on ISAS fields. The uncertainty on TSG data is usually around 0.01–0.02 and is much less compared to the satellite uncertainty and thus is not taken into account in the comparisons. ISAS maps include an estimation of the error, expressed as percentage of a priori variance. But we did not find any relationship between the error in ISAS and the statistics of our colocations.

4. Results

4.1. Colocated SMOS and TSG Data

An illustration of colocation between SMOS SSS and TSG SSS is presented during October 2011 (Figure 5). SMOS SSS (blue curve) was collocated at TSG SSS original resolution (orange curve). In order to allow the comparison at the same scale, TSG SSS was also filtered at the same resolution as SMOS (± 50 km, red line). This TSG transect crosses the SSS maximum from the north-east to its center around 26°N. During October 2011, the RMSE between SMOS and in situ SSS is 0.13, and the corresponding correlation is $r = 0.93$. At large scale, the northward decrease of SSS associated with the northern flank of SSM region (varying from 37.7 to 36.5) is quantitatively well reproduced.

Some mesoscale features (~ 100 km) are relatively well captured in SMOS data, for instance, from 20 to 21 October 2011, but discrepancies are also observed, as on 23 October 2011. Indeed, discrepancies could be due to rapid variability of the small-scale SSS features because of the different space and time sampling of the instantaneous TSG data and the ± 9 days, ± 50 km SMOS data.

More generally, the colocations of SMOS SSS were made for the 39 transects of ship TSG SSS over the period June 2010 to December 2012. The RMSE between SMOS and in situ SSS at 100 km resolution is 0.17 and the correlation is $r = 0.90$ (Table 2). The correlations between SMOS SSS and TSG SSS were degraded by

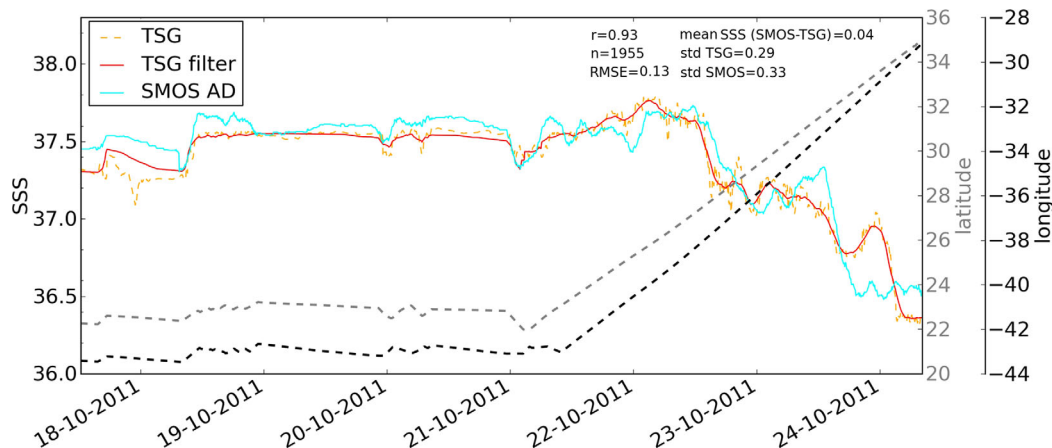


Figure 5. Colocation of SMOS SSS (blue) and SSS from Toucan TSG ship (red for filtered data and orange for nonfiltered data) in October 2011. The applied bias correction is $B1 = -0.172$. The dashed gray curve indicates the latitude value along the transect.

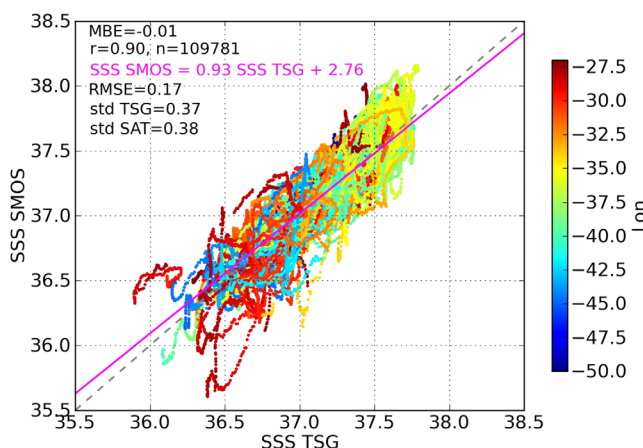


Figure 6. Comparison of SMOS SSS with TSG SSS from all ship transects (Toucan, Colibri, AMT, Rapid, Knorr, and Thalassa) from January 2010 to December 2012. In color, the longitudinal position of each value. SMOS SSS is averaged over 18 days and $100 \times 100 \text{ km}^2$; ship data are filtered over 100 km. A linear regression curve is indicated in red.

using only ascending orbits or descending orbits. Thus, in the following, we will always consider the products that combine the two orbits A and D.

The SSS variability at scale smaller than 100 km is of typically 0.2, up to 0.5, as sampled by in situ measurements (Figure 5) [see also *Delcroix et al.*, 2005, Figures 19 and 21]. In order to filter out this variability, we average TSG SSS over 100 km; however, this does not fully remove this small-scale variability, as this smoothing is 1-D while the satellite smoothing is 2-D. Nevertheless, we observe that this smoothing

only very slightly improves the global ship-satellite SSS comparisons (Table 2), but reduces some local differences by 0.2 or even more (Figure 5).

The comparison of SMOS SSS with TSG SSS from all ship transects (Figure 6) indicates that high differences are observed at the easternmost longitudes corresponding to positions closer to a coast. Thus, the area is probably still affected by the presence of RFI or land contamination. Indeed, inside the NSA area, the north-eastern part of the selected region (Figure 2) displays a quite large variability.

Monthly statistics were also analyzed. The mean difference between SMOS SSS and TSG SSS ranges within ± 0.2 with an uncertainty up to 0.3 (Figure 7). The monthly correlations between TSG SSS and colocated SMOS SSS are generally higher than $r = 0.81$, except during November and December 2012 (Figure 7; colored dots). During these periods, the SMOS SSS data are associated with the most substantial bias corrections, higher than $r = 0.23$ (Figure 7; blue shaded period).

These winter periods were also associated with a smaller amount of valid SMOS SSS observations, and hence a higher level of noise in the averaged SSS. Almost all SMOS Level 2 data on descending orbits during boreal winter (November to January) are flagged due to bad retrieval quality. The averaged salinity is thus derived from data acquired during ascending orbits only. The absence of good quality data on descending orbits is likely due to the effect of sun aliasing over the FOV.

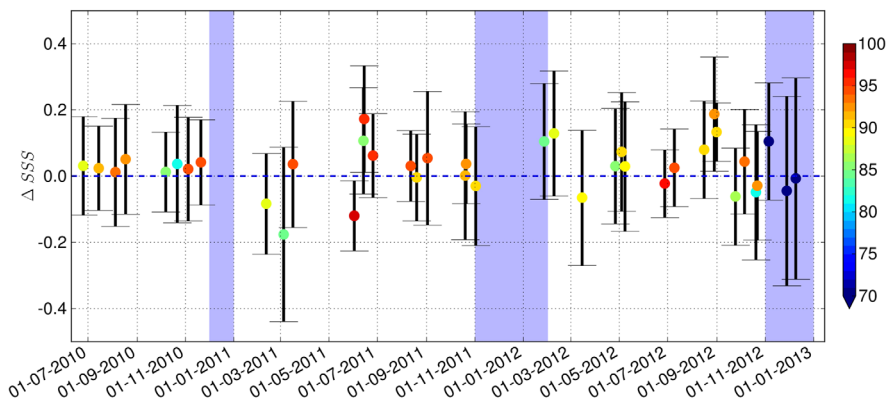


Figure 7. Mean and standard deviation of SSS SMOS-SSS TSG for each TSG section (Colibri, Toucan, AMT, Rapid, Knorr, and Thalassa). Values of correlation coefficient ($r \times 100$) between SSS SMOS and SSS TSG are indicated by color dots. Mean bias correction is applied for each month. Blue shaded strips indicate the periods when the bias corrections is higher than 0.23 (Figure 3). SMOS SSS is averaged over 18 days and $100 \times 100 \text{ km}^2$; ship data are filtered over 100 km.

Table 3. Statistics at $0.25^\circ \times 0.25^\circ$ Resolution, $n = 2404$, $\sigma_{TSG} = 0.37$ Over the Period Common to SMOS and Aquarius From September 2011 to December 2012^a

SSS Products	r	RMSE	σ_p	$y = ax + b$
CEC LOCEAN	0.92 [0.93] (0.92)	0.15 (0.14)	0.37	$y = 0.93x + 2.45$
LOCEAN 0.25°	0.86 [0.88] (0.93)	0.21 (0.14)	0.40	$y = 0.94x + 2.17$
LOCEAN OI	0.94 [0.93] (0.94)	0.13 (0.12)	0.35	$y = 0.89x + 3.93$
CEC IFREMER	0.85 [0.86] (0.88)	0.21 (0.18)	0.36	$y = 0.84x + 5.95$
ISAS	0.93 [0.93] (0.93)	0.14 (0.13)	0.36	$y = 0.9x + 3.76$
AQ V2	0.93 (0.93)	0.14 (0.14)	0.37	$y = 0.93x + 2.48$
AQ V2CAP	0.93 (0.92)	0.14 (0.15)	0.38	$y = 0.95x + 1.73$

^aIn brackets, the correlation coefficient computed using all data from July 2010 ($n = 4238$). In parentheses, the correlation between TSG and SSS products gridded at $1^\circ \times 1^\circ$ resolution ($n = 604$). In gray, data sets with the smallest RMSE and higher Pearson correlation (r).

4.2. Large-Scale Variability

In order to compare performances of SMOS SSS with respect to other SSS products, and given that some of them are only available as monthly maps, we now compare ship SSS with monthly SSS products only collocated in space. When doing so, collocation in time is much less precise and SMOS SSS is much smoother than in the collocations described in section 4.1. As a consequence, the correlation between monthly SMOS SSS and in situ SSS is slightly higher, the RMSE slightly smaller but the slope of the linear fit is less than 1 (first line of Table 3 compared with second line of Table 2 and Figure 6 with Figure 8). The RMSE between in situ SSS and either SMOS CEC LOCEAN, two versions of Aquarius or ISAS is between 0.14 and 0.15 (Table 3). The corresponding correlation coefficients for all these products are between $r = 0.92$ – 0.93 . For SSS products, which had lower nominal resolution than 0.25° , no significant statistical differences were observed between 0.25° and 1° . As expected, the LOCEAN 0.25° product averaged at 100 km resolution is roughly equivalent to SMOS CEC LOCEAN at 1° resolution.

LOCEAN 0.25° SSS presents a worse correlation coefficient than SMOS CEC LOCEAN ($r = 0.86$ instead of $r = 0.92$), indicating that the decrease in SSS natural variability between 0.25° and 100 km is smaller than the noise decrease on SMOS SSS between 0.25° and 100 km. The correlation coefficient of SMOS CEC IFREMER also increases when averaged at 1° . Nevertheless, this product presents a correlation coefficient lower than the one of the other products, likely due to the $5^\circ \times 5^\circ$ bias correction with respect to the climatology that artificially modify the spatial distribution of SSS. Hence, this product will not be used for further analysis.

The comparison between SMOS CEC LOCEAN monthly composite and TSG SSS is shown in Figure 8. The RMSE and correlation coefficients are very similar for SMOS CEC LOCEAN, LOCEAN OI, Aquarius, and ISAS products. Nevertheless, the variance of the SSS products (see standard deviation) and the equation of the

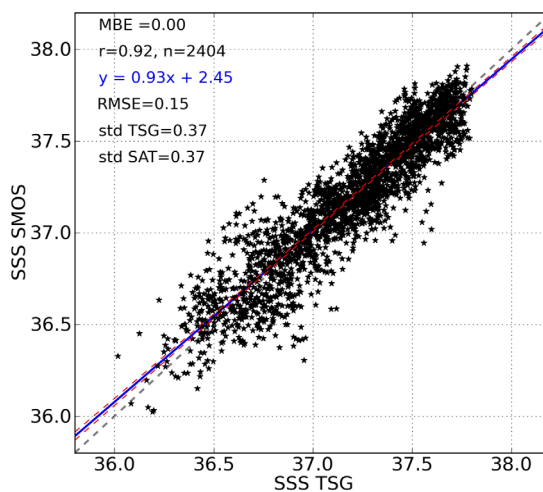


Figure 8. Comparison of SMOS CEC LOCEAN monthly SSS maps with TSG SSS. SMOS CEC LOCEAN SSS averaged over $100 \times 100 \text{ km}^2$ and oversampled every 0.25° . Ship TSG data are averaged over the same SMOS grid of $0.25^\circ \times 0.25^\circ$ resolution. Red line indicates the confidence interval at 95% of linear regression. Data from September 2011 to December 2012 and over the region 50°W – 27°W , 15°N – 35°N .

linear regression are quite different; OI and ISAS have a smaller slope and variance than SMOS and Aquarius. Variance of SMOS CEC LOCEAN and Aquarius is slightly higher than the one of TSG SSS (see Tables 2 and 3), mostly because of noisier satellite SSS than TSG SSS, although near-surface processes or small horizontal scales could also contribute to the higher variance.

While RMSE and correlation are equivalent between these products for the large-scale variability, these products appear to behave quite differently from month to month (not shown). October 2011, where SSS

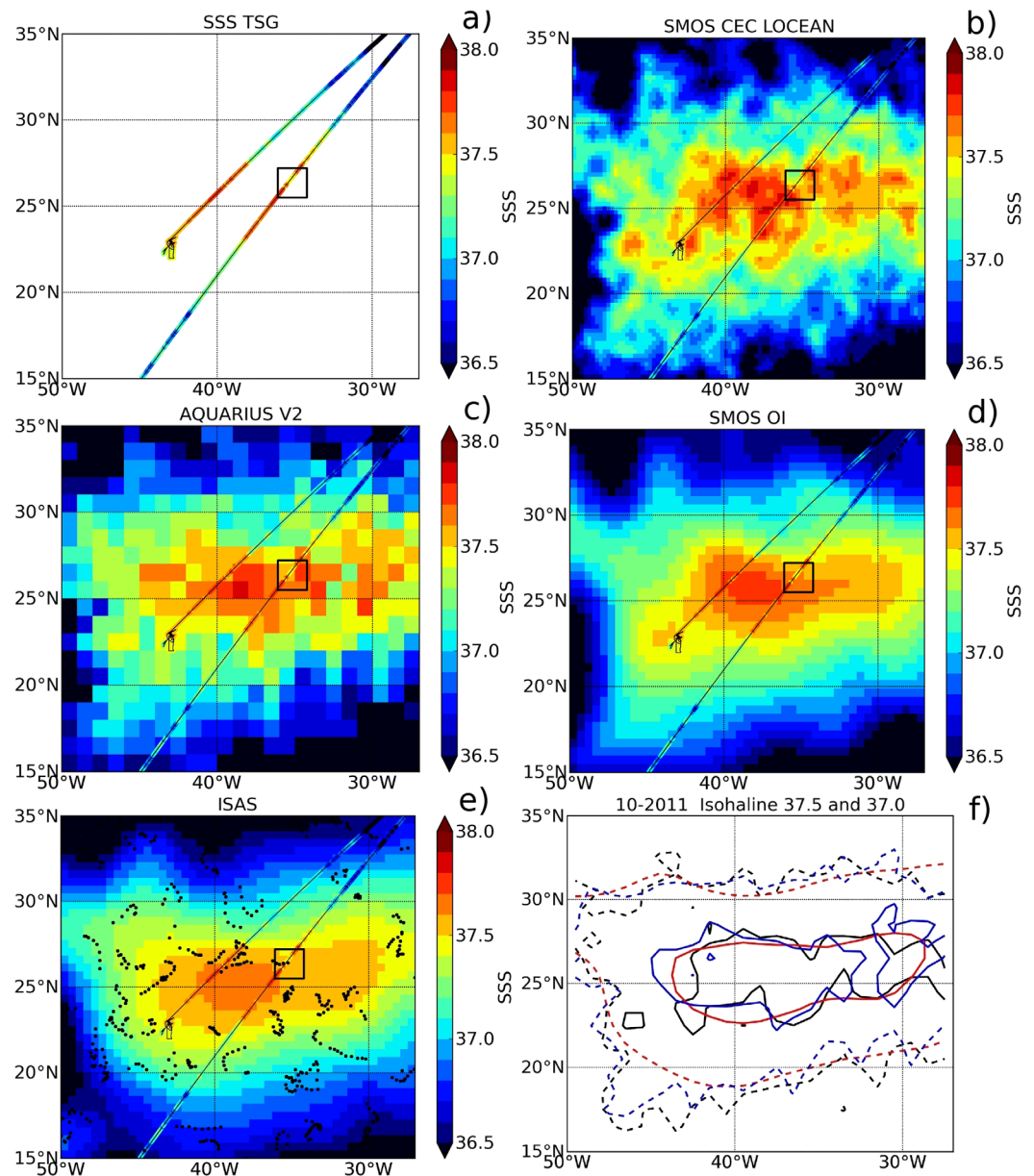


Figure 9. SSS maps for October 2011 from (a) TSG ship, (b) SMOS CEC LOCEAN, (c) Aquarius V2, (d) SMOS OI, and (e) ISAS. Black points indicate the position of Argo floats used in the ISAS analysis for October 2011 (Figure 9e). SSS from ships (Table A1) is superimposed in color over SSS maps (Figures 9b–9d). During October 2011, the applied bias correction is $B1 = -0.172$. (Figure 9f) Isohaline contours (37.5 plain line, 37.0 dashed line) derived from ISAS (red), Aquarius V2 (blue), and SMOS (black). Black square for the region bound within 35.8°W – 34.2°W and 25.2°N – 27.2°N .

presents high spatial variability (Figure 9), has been selected to illustrate the difference between these products. During that month, large-scale SSS signatures (>300 km) are in agreement between SMOS, Aquarius and ISAS (Figure 9). However, within the black square (Figure 9), a southward intrusion of fresher surface water is observed along with a sharp horizontal SSS gradient at scale of about 1° . These small-scale features are clearer in TSG data maps than in the other SSS products, which suggest the ability of SMOS to detect small-scale features of scales less than 300 km.

In order to compare the location of the extension of the SSM region in the NSA region, we compare the 37.5 isohaline (Figure 9f). The isohaline location is to first order in good agreement between the various products at scales down to about 100 km.

To quantify the temporal variability of this SSS maximum location, we estimate the barycenter in the NSA region between 18°N and 33°N (Figure 10, equation (B6)), from the various product at 0.25° resolution. The

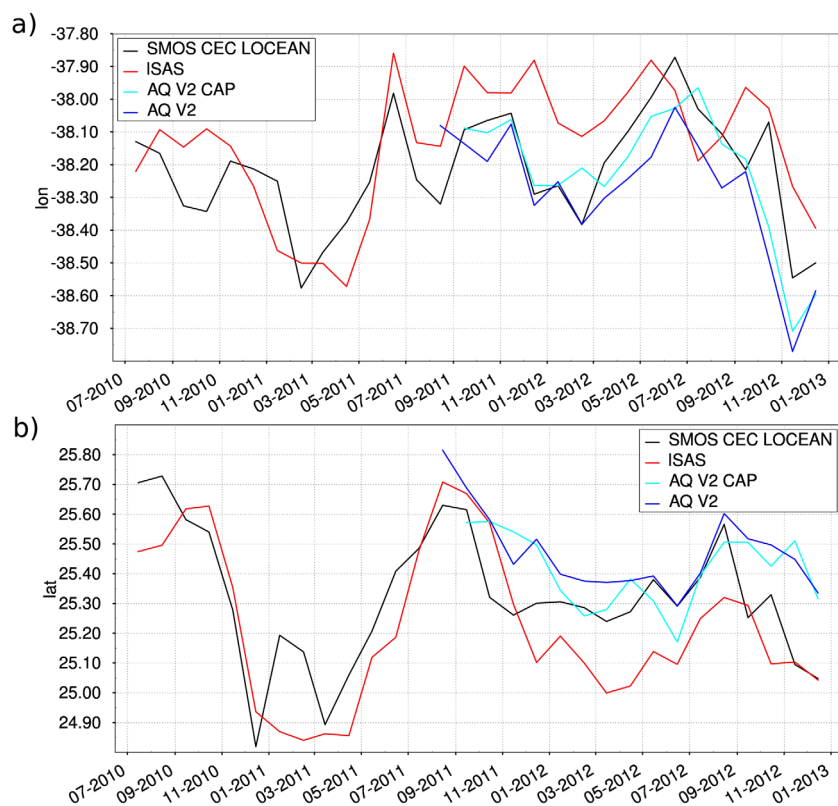


Figure 10. (a) Longitude and (b) latitude of the barycenter of the sea surface salinity maximum for SMOS CEC LOCEAN, ISAS, Aquarius V2, and Aquarius V2 CAP from July 2010 to December 2012. Barycenter computed over the region 50°W – 27°W , 15°N – 35°N .

latitudinal position of the SSS maximum follows a seasonal cycle ($\sim 0.7^{\circ}$ of amplitude; Figure 10b). The most northern (southern) position is reached during summer (spring). No significant seasonal cycle is observed in longitude (Figure 10a). The apparent seasonal latitudinal migration of the SSM is explained by the seasonal variability of the atmospheric and oceanic process [Qu *et al.*, 2011]. During winter, the northern part of the SSM is eroded by the vertical entrainment mixing due to enhanced winter buoyancy loss [Vinogradova and Ponte, 2013; N. Kolodziejczyk *et al.*, SMOS salinity in the subtropical North Atlantic salinity maximum: 2. Bi-dimensional horizontal thermohaline variability, submitted to *Journal of Geophysical Research: Oceans*, 2014], while during summer, south of the SSM, both advection of freshwater from Amazon-Orinoco runoff and higher precipitation due to ZTIC northward migration produces a freshening of the southern part of the SSM [Vinogradova and Ponte, 2013].

4.3. Mesoscale Features

In order to further investigate the capability of various products to measure the small-scale variability, we remove the large-scale variability. For this, the ISAS climatological mean is removed from each satellite product as well as the ISAS product. The resulting fields of SSS anomalies during October 2011 are shown in Figure 11. The TSG, SMOS, and Aquarius SSS anomalies show SSS spatial variability to be within ± 0.6 (Figures 11a–11c), with a scale of ~ 100 km. Both ISAS and SMOS OI SSS anomalies present spatial SSS features at a scale of ~ 300 km (Figure 11e), which comes from interannual SSS variability; the difference between ISAS and SMOS OI is mainly due to Argo coverage (Figure 11d).

The spatial structures of SMOS and Aquarius SSS anomalies are in a reasonable agreement with TSG anomalies (Figures 11b and 11c). Nevertheless Aquarius SSS anomalies are in general significantly smaller than SMOS. In the south-western domain (around 22°N and 49°W), strong negative SSS anomalies (< 0.5) and sharp SSS gradient are likely due to the intrusion of freshwater coming from the Amazon discharge [Reul *et al.*, 2013]. In the north-western quarter of the domain, positive SSS anomalies (> 0.3) are also seen with both satellites (around positions centered at 26°N – 40°W ; 30°N – 40°W ; and 33°N – 45°W). Furthermore, the SMOS and Aquarius SSS anomalies are in good agreement with TSG SSS anomalies along the ship tracks. However, the best visual agreements is seen comparing the TSG and the SMOS SSS anomalies (Figures 11a–11c).

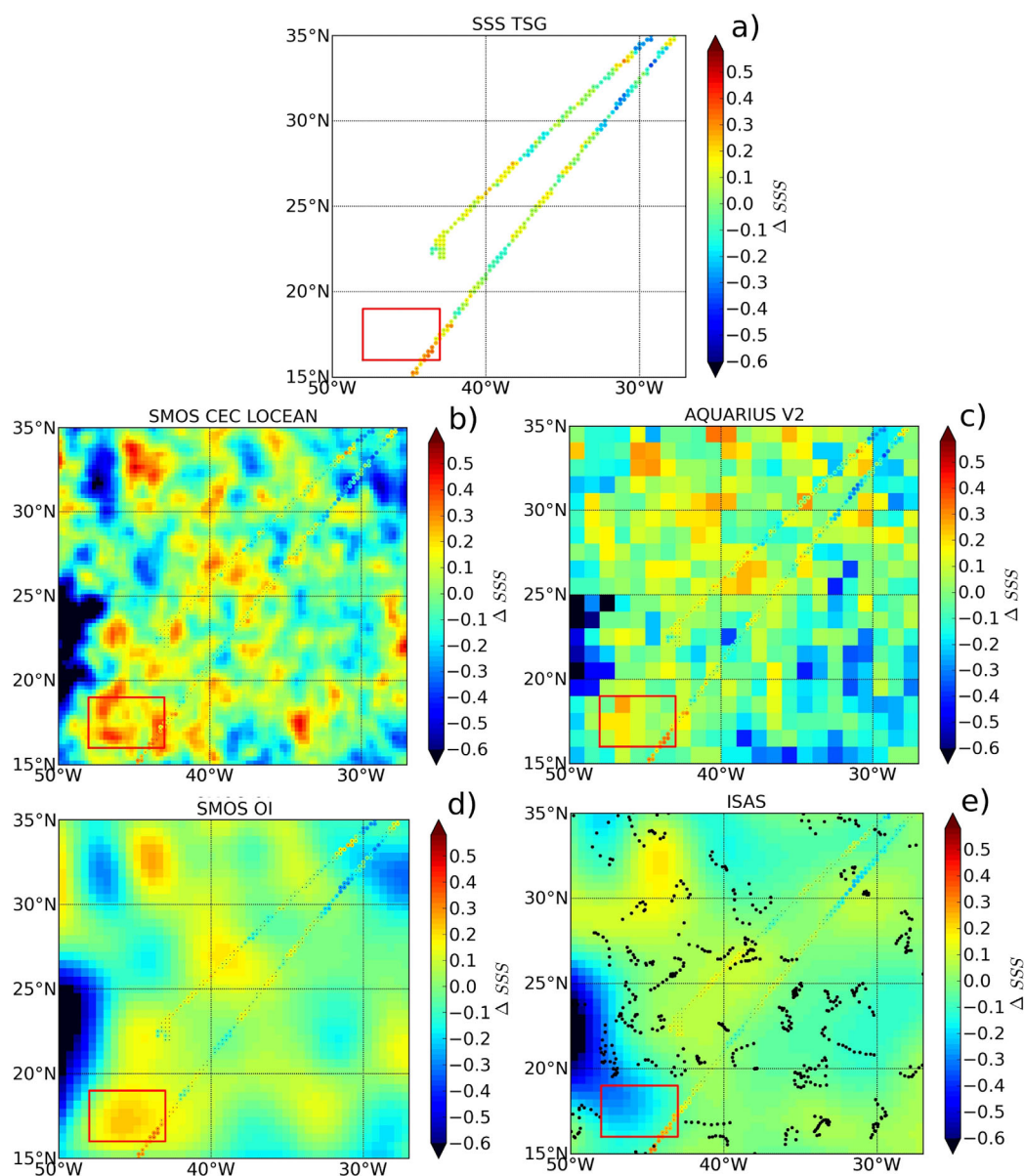


Figure 11. SSS anomaly maps for October 2011 from (a) TSG ship, (b) SMOS CEC LOCEAN, (c) Aquarius V2, (d) SMOS OI, and (e) ISAS. Black points indicate the position of Argo floats used in the ISAS analysis for October 2011 (Figure 11e). SSS from ships (Table A1) is superimposed in color over SSS maps (Figures 11b–11e). For SMOS OI and ISAS, the ship SSS has been previously filtered at 300 km. Red square for the region bound within 48°W–43°W and 16°N–19°N.

The comparison between SMOS OI and ISAS OI SSS anomalies also shows large differences that are likely due to the sparse spatial coverage of Argo. For instance, in the south-western part, the SSS fresh anomalies due to the Amazon freshwater plumes extend too far east in the ISAS OI products (around 17°N–47°W), and that product does not reproduce the positive SSS anomaly seen by TSG data in the red square of Figure 11, contrary to satellite products. Indeed, there is no Argo data at that time in this area. This demonstrates that the better coverage obtained from satellite data allows a more accurate representation of the SSS meso-scale features, particularly in regions of strong SSS gradients.

In order to systematically validate the mesoscale features from satellite data, the correlation between SSS anomalies from satellite and the 39 collocated TSG sections SSS anomalies have been computed (Figure 12). SMOS SSS and Aquarius SSS are significantly correlated (significant at 99%) with TSG SSS anomalies with correlation coefficients of $r = 0.57$ for SMOS, $r = 0.52$ for Aquarius V2,

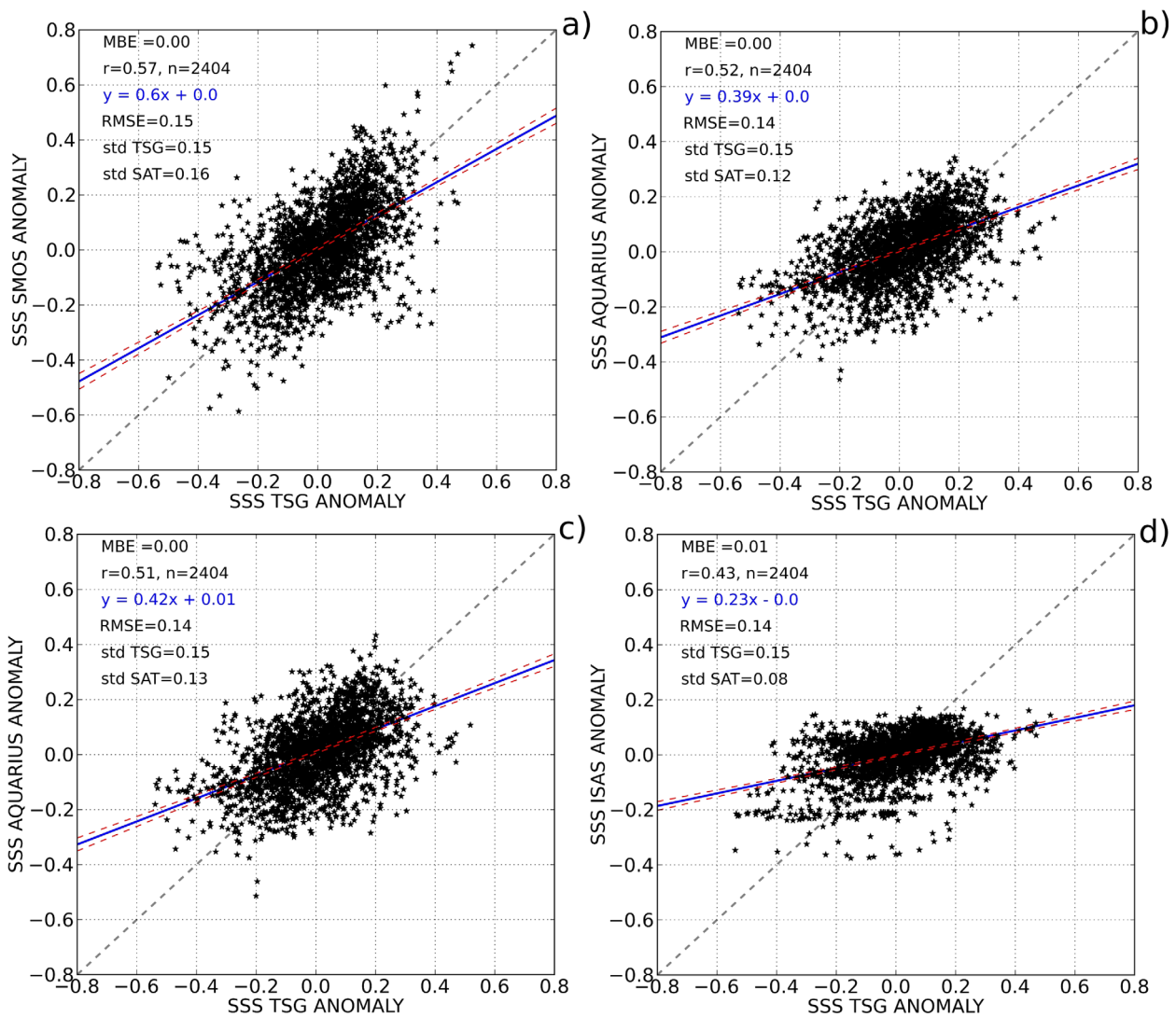


Figure 12. Comparison of (a) SMOS CEC LOCEAN SSS anomaly, (b) Aquarius V2 SSS anomaly, (c) Aquarius V2 CAP SSS anomaly, and (d) ISAS SSS anomaly with TSG SSS anomaly at 0.25° grid resolution. Red line indicates the confidence interval at 95% of linear regression. Data from September 2011 to December 2012 and over the region 50°W–27°W, 15°N–35°N.

$r = 0.51$ for Aquarius V2CAP, and $r = 0.39$ for ISAS (Figure 11 and Table 4). The Fisher r-to-z transformation showed that the differences in correlation coefficient were significant at 95% between SMOS, ISAS, and Aquarius, but not between the two versions of Aquarius. SMOS SSS presents a higher correlation than the other products as well as higher variance, thus potentially portraying more signal. On the other hand, the $3^\circ \times 3^\circ$ resolution ISAS product is not expected to be well correlated with the TSG. When SMOS is averaged at the same space and time scale as Aquarius ($1^\circ \times 1^\circ$, 1 month; Table 4), the correlation coefficient is still significantly higher. Also, the slope of the linear regression in SMOS is higher, indicating that values of SMOS SSS anomalies are in better agreement with TSG SSS anomalies. These results suggest that SMOS SSS best represent mesoscale features in the analyzed region and time period.

Results of SMOS and ISAS statistics remain very similar using 18 supplementary transects (from January 2010 to August 2011; see Table 4). The effect of better spatial and temporal sampling of SMOS with respect to Argo data is studied by comparing the 39 TSG sections SSS anomalies filtered at 300 km (the nominal resolved resolution of the interpolated products) with the SMOS OI and the ISAS SSS anomalies. The correlation coefficient is better with the SMOS OI SSS anomalies than with ISAS (Figure 13 and Table 5):

$$r_{SMOS} = 0.66, r_{ISAS} = 0.55.$$

Table 4. Statistics of SSS Anomalies of SMOS CEC LOCEAN, ISAS, and Aquarius With Respect to TSG SSS Anomaly Over the Overlapping Period of SMOS and Aquarius From September 2011 to December 2012, n = 2404^a

	r	RMSE	σ_{TSG}	σ_p	y = ax + b
CEC LOCEAN	0.57 [0.58] (0.56)	0.15 (0.14)	0.15	0.16	y = 0.60 (0.63) x + 0.00
AQ V2	0.52 (0.52)	0.14 (0.14)	0.15	0.12	y = 0.39 (0.49) x + 0.01
AQ V2CAP	0.51 (0.48)	0.14 (0.15)	0.15	0.13	y = 0.42 (0.49) x + 0.01
ISAS	0.43 [0.44] (0.44)	0.14 (0.13)	0.15	0.08	y = 0.23 (0.24) x - 0.00

^aAll SSS products as well as TSG are binned at 0.25°. In brackets, the correlation coefficient computed using data from July 2010 (n = 4238). In parentheses, the correlation obtained by gridding TSG and SSS products at 1° × 1° resolution (n = 604).

5. Discussion and Conclusion

SMOS SSS products have been compared with ship TSG SSS data in the NAS SSM region between June 2010 and December 2012. By comparing satellite SSS with objectively analyzed in situ data (ISAS), a seasonal bias in satellite SMOS SSS is observed with a strong negative bias during the boreal winter (up to 0.4). In this study, we mainly focus on the capability of SMOS products to measure spatial variability of the SSS field, so the monthly bias is first corrected by removing the monthly mean difference between SSS computed for each SSS satellite product (SMOS or Aquarius) with ISAS over the whole NSA region. Since bias correction is done using a regional average of the ISAS SSS climatology, which includes no TSG SSS data, there may be a residual error, which would correspond to the difference between ISAS and ship SSS.

To first order and very large scale, the spatial distribution of the sea surface salinity maximum is quite consistent between SMOS, Aquarius, and ISAS. The correlation coefficients between ship SSS and these monthly SSS products are r = 0.92–0.93 with a RMSE of 0.14–0.15. The latter is well below the SSS variability observed by ship SSS (about 0.4; see Table 4). These performances are close to the ones observed by *Hasson et al.* [2013] in the maximum salinity region of the South Pacific, demonstrating a great potential of new satellite SSS products for studying salinity variability and associated processes in subtropical regions.

The comparison between SMOS SSS monthly products and synoptic ship SSS was expected to be less relevant than the ±9 days collocations, but they are also less noisy. Indeed, in spite of a partial loss of time consistency with the use of the monthly SMOS SSS, the statistics (correlation coefficient and RMSE) are improved. However, as indicated by the smaller SMOS-to-TSG SSS slope of the linear fitting, some signal has been lost with monthly smoothing. It is thus worth noticing that monthly smoothing of the SMOS SSS improves the signal-to-noise ratio.

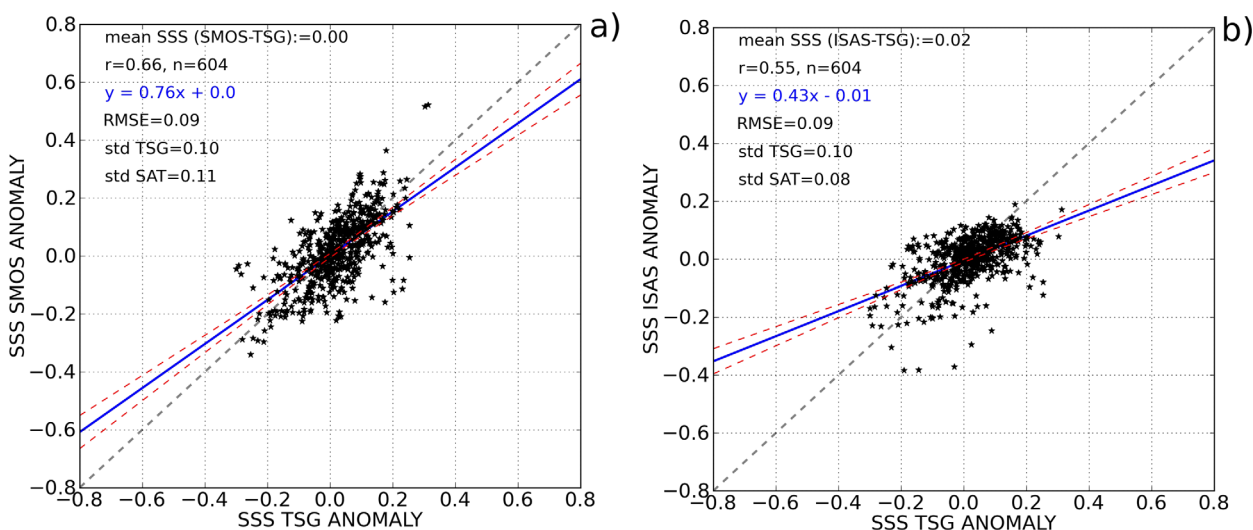


Figure 13. Comparison of (a) SMOS OI SSS anomaly and (b) ISAS SSS anomaly with TSG SSS anomaly filtered at 300 km and binned at 1° grid resolution. Red line indicates the confidence interval at 95% of linear regression. Data from September 2011 to December 2012 and over the region 50°W–27°W, 15°N–35°N.

Table 5. Statistics of SSS Anomaly of LOCEAN OI SSS and ISAS SSS With Respect to TSG SSS Anomaly Filtered at 300 km on a $1^\circ \times 1^\circ$ grid, $n = 604$.

	r	RMSE	σ_{TSG}	σ_p	y = ax + b
LOCEAN OI	0.66	0.09	0.10	0.11	y = 0.76x + 0.01
ISAS	0.55	0.09	0.1	0.08	y = 0.43x - 0.01

The synoptic coverage of satellite data makes it possible to investigate salinity in regions where Argo network poorly resolves the variability, especially, in the region of the Amazon-Orinoco plume. This region presents a very sharp gradient of SSS between the freshwater plume and the subtropical SSS maximum, with large spatiotemporal variability [Reverdin *et al.*, 2007; Reul *et al.*, 2013; Grodsky *et al.*, 2014]. SMOS provides SSS information that well-complement Argo profiles as it better documents the spatial extent of the freshwater plume (Figure 11). The Amazon-Orinoco surface freshwater overlaying the subsurface high salinity waters contributes to the formation and variability of the barrier layer [de Boyer Montégut, 2004; Tanguy *et al.*, 2010; Mignot *et al.*, 2012; Grodsky *et al.*, 2012]. This barrier layer likely plays an important role in the ocean-atmosphere interaction in the tropics [Balaguru *et al.*, 2012].

At mesoscales, satellite products provide quite reliable information on SSS spatial features at scales of ~ 100 km. Correlation coefficients with TSG SSS anomalies are $r = 0.57$ for SMOS SSS anomalies, $r = 0.52$ for Aquarius SSS anomalies, and $r = 0.43$ for ISAS SSS anomalies. In spite of a remaining high level of noise and caveats in the retrieval process, it is the first time that satellite SSS products resolved ~ 100 km resolution scale. These mesoscale features are consistently detected by both SMOS and Aquarius.

These features are likely remnants of salty surface eddies, meanders of SSS fronts, and provide for the first time the opportunity to investigate the thermohaline structures of ocean surface in the subtropical and tropical Atlantic via satellite measurements (see Kolodziejczyk *et al.*, submitted manuscript, 2014, companion paper). These issues are crucial in order to better understand impacts of surface thermohaline properties in the regions of Atlantic subtropical water subduction during the boreal winter [e.g., Iselin, 1939; Schmitt, 1999; Johnson *et al.*, 2012].

These correlations vary significantly at monthly time scales and SMOS provides SSS information particularly interesting for summer period. ISAS SSS anomalies exhibit always low correlation coefficient values (around $r = 0-0.2$) during summer contrary to SMOS SSS anomalies (about $r = 0.6$). Summer months correspond to the time period when the SSS variability on the NSA region reaches its maximum (Figure 3a), probably corresponding also to the higher mesoscale variability and higher SSS gradients.

In contrast, in winter, a higher SSS bias and lower correlation are observed with SMOS SSS, when very few SMOS SSS are accurately retrieved in the Northern Hemisphere on descending orbits likely due to remaining solar radiation impacts in the SMOS data.

In spite of larger level of noise in individual satellite measurements compared with in situ measurements, satellite products are shown to be able to better reproduce SSS mesoscale variability than interpolated in situ data. This can be understood because of the better synoptic coverage of satellite data. In this study, we quantify for the first time this effect.

Furthermore SMOS data are found to present a better agreement with observations than Aquarius in the analyzed region and time period. These two satellites differ in the technology used; hence both satellites complement each other, SMOS providing higher spatial and temporal resolution (3–5 days, 43 km for SMOS versus 7 days and 100 km for Aquarius), a much better ocean coverage (swath width larger than 600 km for SMOS, about 300 km for Aquarius) while the precision on single retrieved SSS is much better with Aquarius than with SMOS (about a factor of 2–3). We find that Aquarius provides less seasonal bias on regional SSS; after averaging SSS data over 100 km and 1 month and correcting for large-scale seasonal biases, SMOS SSS better captures the spatial scale variability, partly due to its better space and time sampling.

The objective of the SMOS mission is to achieve 0.1 accuracy on the SSS averaged over 100 km and 1 month. Actually, after locally correcting a monthly bias, we found an accuracy of monthly SSS at 100 km resolution of about 0.15 and a correlation of $r = 0.92$ with in situ data. Research is still ongoing to improve SMOS Tb calibration image reconstruction and RFI filtering that should help to reduce seasonal biases and improve local SSS, but this remains a challenging task.

Appendix A: Additional Data

Table A1 shows the TSG data used in the study.

Table A1. Merchant Sips (Colibri and Toucan) TSG Transects, AMT, Rapid, Knorr, and Thalassa transect^a

Ship Name	Start Date	End Date
Toucan	22 Jun 2010	27 Jun 2010
Toucan	12 Jul 2010	17 Jul 2010
Colibri	2 Aug 2010	6 Aug 2010
Colibri	15 Aug 2010	19 Aug 2010
Colibri	5 Oct 2010	7 Oct 2010
Colibri	19 Oct 2010	24 Oct 2010
Toucan	3 Nov 2010	5 Nov 2010
Toucan	19 Nov 2010	22 Nov 2010
Toucan	1 Feb 2011	19 Feb 2011
Colibri	2 Mar 2011	6 Mar 2011
Colibri	15 Mar 2011	19 Mar 2011
Toucan	30 May 2011	3 Jun 2011
Toucan	12 Jun 2011	14 Jun 2011
Colibri	11 Jun 2011	15 Jun 2011
Colibri	24 Jun 2011	28 Jun 2011
Colibri	9 Aug 2011	13 Aug 2011
Toucan	17 Aug 2011	21 Aug 2011
Toucan	29 Aug 2011	5 Sep 2011
Toucan	17 Oct 2011	24 Oct 2011
Colibri	17 Oct 2011	21 Oct 2011
Colibri	30 Oct 2011	4 Nov 2011
Colibri	25 Jan 2012	29 Jan 2012
Colibri	6 Feb 2012	11 Feb 2012
Colibri	13 Mar 2012	17 Mar 2012
Colibri	24 Apr 2012	28 Apr 2012
Toucan	1 May 2012	6 May 2012
Colibri	6 May 2012	10 May 2012
Toucan	25 Jun 2012	29 Jun 2012
Toucan	7 Jul 2012	11 Jul 2012
Toucan	13 Aug 2012	18 Aug 2012
Thalassa	18 Aug 2012	12 Sept 2012
Toucan	26 Aug 2012	31 Aug 2012
Knorr	10 Sept 2012	8 Oct 2012
Toucan	4 Oct 2012	7 Oct 2012
AMT	17 Oct 2012	26 Oct 2012
Toucan	18 Oct 2012	22 Oct 2012
Rapid	1 Nov 2012	9 Nov 2012
Colibri	26 Nov 2012	30 Nov 2012
Colibri	7 Dec 2012	11 Dec 2012

^aFirst column indicates the name of the ship; second and third columns indicate the start date and the end date of the transect within NSA region (50°W–27°W, 15°N–35°N).

Appendix B: Statistical Equations

The correlation coefficient *r* is defined as:

$$r = \left[\frac{1}{n} \frac{\sum_{i=1}^n (P_i - \bar{P})(O_i - \bar{O})}{\sigma_P \sigma_O} \right] \tag{B1}$$

with *P* corresponding to the different SSS products (ISAS, SMOS or Aquarius) and *O* the observed in situ data (TSG ship). σ_P and σ_O are the corresponding standard deviations related to *P* and *O*, respectively. *n* is the total number of observations.

To assess the difference in correlation coefficients between two data sets *r*₁ and *r*₂ of size *n*₁ and *n*₂, we use the fisher *r*-to-*z* transformation [Zar, 2010].

$$z = \left(0.5 \cdot \ln \left(\frac{1+r_1}{1-r_1} \right) - 0.5 \cdot \ln \left(\frac{1+r_2}{1-r_2} \right) \right) \cdot \left(\sqrt{\frac{1}{N_1-3} + \frac{1}{N_2-3}} \right)^{-1} \quad (B2)$$

The root mean square error (RMSE) is defined as:

$$RMSE = \sqrt{\frac{1}{n} \sum_{i=1}^n (P_i - O_i)^2} \quad (B3)$$

The mean bias error (MBE) is defined as:

$$MBE = \frac{1}{n} \left(\sum_{i=1}^n (P_i - O_i) \right) \quad (B4)$$

The standard deviation is defined as:

$$\sigma_P = \sqrt{\frac{1}{n} \sum_{i=1}^n (P_i - \bar{P})^2} \quad (B5)$$

The longitude (lon) and latitude (lat) of the barycenter (B) of the sea surface salinity (SSS) (lon_B , lat_B) are calculated as:

$$lon_B = \sum_{i,j} \frac{SSS_{ij} lon_i}{SSS_{ij}} \quad lat_B = \sum_{i,j} \frac{SSS_{ij} lat_j}{SSS_{ij}} \quad (B6)$$

Acknowledgments

This study is supported by the ESA SMOS+SOS ("OSMOSIX") project. It is part of the ESA SMOS/GLOSCAL Cal/Val project funded by CNES. Sea surface salinity data derived from thermosalinograph instruments installed on board Toucan and Colibri voluntary observing ships were collected, validated, archived, and made freely available by the French Sea Surface Salinity Observation Service (<http://www.legos.obs-mip.fr/observations/sss>, special thanks to Denis Diverres and Stéphane Jacquin). TSG data from R/V Knorr have been provided by Julian Schanze and Ray Schmitt from the SPURS project funded by NSF and NOAA. TSG data from Rapid Cruise (RRS Discovery Cruise 382) and for AMT cruise 22 have been obtained with NERC support and distributed by BODC. Aquarius V2.0 version and Aquarius V2.0 CAP version were obtained from the Physical Oceanography Distributed Active Archive Center (PO.DAAC) at the NASA Jet Propulsion Laboratory, Pasadena, CA, <http://podaac.jpl.nasa.gov>. We thank two anonymous reviewers for their constructive remarks and Gary Lagerloef for his advices about Aquarius data.

References

- Balaguru, K., P. Chang, R. Saravanan, and C. J. Jang (2012), The barrier layer of the atlantic warm pool: Formation mechanism and influence on the mean climate, *Tellus, Ser. A*, *64*, 18162, doi:10.3402/tellusa.v64i0.18162.
- Bingham, F. M., G. R. Foltz, and M. J. McPhaden (2012), Characteristics of the seasonal cycle of surface layer salinity in the global ocean, *Ocean Sci.*, *8*(5), 915–929, doi:10.5194/osd-8-2377-2011.
- Boutin, J., N. Martin, G. Reverdin, X. Yin, and F. Gaillard (2013), Sea surface freshening inferred from SMOS and Argo salinity: Impact of rain, *Ocean Sci.*, *9*, 183–192, doi:10.5194/os-9-183-2013.
- Boyer, T. P., and S. Levitus (2002), Harmonic analysis of climatological sea surface salinity, *J. Geophys. Res.*, *107*(C12), 8006, doi:10.1029/2001JC000829.
- Conkright, M., and T. Boyer (2002), *World Ocean Atlas 2001: Objective Analyses, Data Statistics, and Figures* [CD-ROM], 17 pp., Natl. Oceanogr. Data Cent., Silver Spring, Md.
- Curry, R., B. Dickson, and I. Yashayaev (2003), A change in the freshwater balance of the atlantic ocean over the past four decades, *Nature*, *426*(6968), 826–829, doi:10.1038/nature02206.
- Dai, A., and K. E. Trenberth (2002), Estimates of freshwater discharge from continents: Latitudinal and seasonal variations, *J. Hydrometeorol.*, *3*(6), 660–687, doi:10.1175/1525-7541(2002)003<0660:EOFDFC>2.0.CO;2.
- de Boyer Montégut, C. (2004), Mixed layer depth over the global ocean: An examination of profile data and a profile-based climatology, *J. Geophys. Res.*, *109*, C12003, doi:10.1029/2004JC002378.
- Delcroix, T., M. McPhaden, A. Dessier, and Y. Gouriou (2005), Time and space scales for sea surface salinity in the tropical oceans, *Deep Sea Res., Part I*, *52*(5), 787–813, doi:10.1016/j.dsr.2004.11.012.
- Durack, P. J., and S. E. Wijffels (2010), Fifty-year trends in global ocean salinities and their relationship to broad-scale warming, *J. Clim.*, *23*, 4342–4362, doi:10.1175/2010JCLI3377.1.
- Font, J., A. Camps, A. Borges, M. Martin-Neira, J. Boutin, N. Reul, Y. Kerr, A. Hahne, and S. Mecklenburg (2010), SMOS: The challenging sea surface salinity measurement from space, *Proc. IEEE*, *98*(5), 649–665, doi:10.1109/JPROC.2009.2033096.
- Gaillard, F. (2012), ISAS-Tool Version 6: Method and configuration, Ifremer, 18 pp., France, doi:10.13155/22583.
- Gaillard, F., E. Autret, V. Thierry, P. Galaup, C. Coatanoean, and T. Loubrieu (2009), Quality control of large Argo datasets, *J. Atmos. Oceanic Technol.*, *26*, 337–351, doi:10.1175/2008JTECHO552.1.
- Gordon, A., and C. Giulivi (2008), Sea surface salinity trends over fifty years within the subtropical north Atlantic, *Oceanography*, *21*(1), 20–29, doi:10.5670/oceanog.2008.64.
- Grotsky, S. A., N. Reul, G. Lagerloef, G. Reverdin, J. A. Carton, B. Chapron, Y. Quilfen, V. N. Kudryavtsev, and H.-Y. Kao (2012), Haline hurricane wake in the Amazon/Orinoco plume: Aquarius/SACD and SMOS observations, *Geophys. Res. Lett.*, *39*, L20603, doi:10.1029/2012GL053335.
- Grotsky, S. A., G. Reverdin, J. A. Carton, and V. J. Coles (2014), Year-to-year salinity changes in the Amazon plume: Contrasting 2011 and 2012 Aquarius/SACD and SMOS satellite data, *Remote Sens. Environ.*, *140*, 14–22, doi:10.1016/j.rse.2013.08.033.
- Hasson, A., T. Delcroix, and J. Boutin (2013), Formation and variability of the south pacific sea surface salinity maximum in recent decades, *J. Geophys. Res. Oceans*, *118*, 5109–5116, doi:10.1002/jgrc.20367.

- Iselin, C. (1939), The influence of vertical and lateral turbulence on the characteristics of the waters at mid-depths, *Trans. AGU*, 20(3), 414–417, doi:10.1029/TR020i003p00414.
- Johnson, G. C., S. Schmidtke, and J. M. Lyman (2012), Relative contributions of temperature and salinity to seasonal mixed layer density changes and horizontal density gradients, *J. Geophys. Res.*, 117, C04015, doi:10.1029/2011JC007651.
- Kerr, Y., et al. (2010), The SMOS mission: New tool for monitoring key elements of the global water cycle, *Proc. IEEE*, 98(5), 666–687, doi:10.1109/JPROC.2010.2043032.
- Klein, L., and C. Swift (1977), An improved model for the dielectric constant of sea water at microwave frequencies, *IEEE J. Oceanic Eng.*, 2(1), 104–111, doi:10.1109/TAP.1977.1141539.
- Kolodziejczyk, N., and F. Gaillard (2013), Variability of the heat and salt budget in the subtropical south-eastern pacific mixed layer between 2004 and 2010: Spice injection mechanism, *J. Phys. Oceanogr.*, 43, 1880–1898, doi:10.1175/JPO-D-13-04.1.
- Lagerloef, G., et al. (2008), The Aquarius/SAC-D mission: Designed to meet the salinity remote-sensing challenge, *Oceanography*, 21(1), 68–81, doi:10.5670/oceanog.2008.68.
- Lagerloef, G. (2012), Satellite mission monitors ocean surface salinity, *Eos Trans. AGU*, 93(25), 233–240, doi:10.1029/2012EO250001.
- Lagerloef, G., et al. (2010), Resolving the Global Surface Salinity Field and Variations by Blending Satellite and In Situ Observations, *OceanObs'09: Sustained Ocean Observations and Information for Society Venice, Italy, 21–25 September 2009*, ESA Publication WPP-306, doi:10.5270/OceanObs09.cwp.51.
- Lagerloef, G., et al. (2010), Resolving the global surface salinity field and variations by blending satellite and in situ observations, in *Proceedings of OceanObs'09*, doi:10.5270/OceanObs09.cwp.51.
- Lagerloef, G., et al. (2013), Aquarius salinity validation analysis, Tech. Rep. AQ-014-PS-0016, NASA, Pasadena, Calif.
- Martin-Neira, M., et al. (2013), SMOS instrument performance and calibration after 3 years in orbit, in *EGU General Assembly Conference Abstracts*, vol. 15, EGU2013-9556.
- McCarthy, G., et al. (2012), RRS Discovery Cruise 382, 08 Oct-24 Nov 2012. RAPID moorings cruise report, Natl. Oceanogr. Cent. Cruise Rep. 21, 196 pp., Natl. Oceanogr. Cent., Southampton, U. K.
- Mecklenburg, S., et al. (2012), ESA's soil moisture and ocean salinity mission: mission performance and operations, *IEEE Trans. Geosci. Remote Sens.*, 50(5), 1354–1366, doi:10.1109/TGRS.2012.2187666.
- Mignot, J., A. Lazar, and M. Lacarra (2012), On the formation of barrier layers and associated vertical temperature inversions: A focus on the northwestern tropical atlantic, *J. Geophys. Res.*, 117, C02010, doi:10.1029/2011JC007435.
- Qu, T., S. Gao, and I. Fukumori (2011), What governs the North Atlantic salinity maximum in a global GCM?, *Geophys. Res. Lett.*, 38, L07602, doi:10.1029/2011GL046757.
- Reul, N., and J. Tenerelli (2011), SMOS level 3 SSS research products: Product validation document reprocessed year 2010, Tech. Doc. CATDS-CECOS-L3-VALDOC, Inst. Fr. de Rech. Pour l'Exploit. de la Mer, Brest, France. [Available at http://www.ifremer.fr/naiad/salinityremotesensing.ifremer.fr/CATDS_CECOS_SMOS_Level3Products_Validation.pdf.]
- Reul, N., et al. (2013), Sea surface salinity observations from space with the SMOS satellite: A new means to monitor the marine branch of the water cycle, *Surv. Geophys.*, 35, 681–722, doi:10.1007/s10712-013-9244-0.
- Reverdin, G., E. Kestenare, C. Frankignoul, and T. Delcroix (2007), Surface salinity in the Atlantic Ocean (30°S–50°N), *Prog. Oceanogr.*, 73, 311–340, doi:10.1016/j.pocean.2006.11.004.
- Schmitt, R. W. (1999), OCEANOGRAPHY: Spice and the demon, *Science*, 283, 498–499, doi:10.1126/science.283.5401.498.
- Tanguy, Y., S. Arnault, and P. Lattes (2010), Isothermal, mixed, and barrier layers in the subtropical and tropical Atlantic ocean during the ARAMIS experiment, *Deep Sea Res., Part 1*, 57(4), 501–517, doi:10.1016/j.dsr.2009.12.012.
- Terray, L., L. Corre, S. Cravatte, T. Delcroix, G. Reverdin, and A. Ribes (2012), Near-surface salinity as nature's rain gauge to detect human influence on the tropical water cycle, *J. Clim.*, 25, 958–977, doi:10.1175/JCLI-D-10-05025.1.
- Vergely, J.-L., F. Rouffi, P. Waldteufel, E. Anterrieu, and I. Corbella (2013), SMOS+ innovation: Polarimetry, *Prod. Validation Rep. ACGRI-ST*, Sophia-Antipolis, France. [Available at <http://smosp.acri.fr/docs/vr.pdf>.]
- Vinogradova, N. T., and R. M. Ponte (2013), Clarifying the link between surface salinity and freshwater fluxes on monthly to interannual time scales, *J. Geophys. Res. Oceans*, 118, 3190–3201, doi:10.1002/jgrc.20200.
- Wentz, F. J., and D. Le Vine (2012), Aquarius salinity retrieval algorithm: Final pre-launch version (Version 2: Algorithm theoretical basis document), *RSS Tech. Rep. 082912*, 45 pp., Remote Sensing System, Santa Rosa, Calif.
- Yin, X., J. Boutin, and P. Spurgeon (2012), First assessment of SMOS data over open ocean: Part I Pacific Ocean, *IEEE Trans. Geosci. Remote Sens.*, 50(5), 1648–1661, doi:10.1109/TGRS.2012.2188407.
- Yin, X., J. Boutin, and P. Spurgeon (2013), Biases between measured and simulated SMOS brightness temperatures over ocean: Influence of sun, *IEEE J. Sel. Topics Appl. Earth Obs. Remote Sens.*, 6(3), 1341–1350, doi:10.1109/JSTARS.2013.2252602.
- Yueh, S., W. Tang, A. Fore, A. Freedman, G. Neumann, J. Chaubell, and A. Hayashi (2012), Simultaneous salinity and wind retrieval using the cap algorithm for Aquarius, paper presented at IEEE International Geoscience and Remote Sensing Symposium, IEEE, Munich, Germany. [Available at <http://www.igarss2012.org/Papers/viewpapers.asp?papernum=1596>.]
- Zar, J. H. (2010), *Biostatistical Analysis*, 5th ed., 944 pp., Pearson, Upper Saddle River, N. J.
- Zine, S., et al. (2008), Overview of the SMOS sea surface salinity prototype processor, *IEEE Trans. Geosci. Remote Sens.*, 46(3), 621–645, doi:10.1109/TGRS.2008.915543.